Soft Matter

PAPER

View Article Online
View Journal

Cite this: DOI: 10.1039/c5sm00155b

Entangled F-actin displays a unique crossover to microscale nonlinearity dominated by entanglement segment dynamics

Tobias T. Falzone, Savanna Blair and Rae M. Robertson-Anderson*

Received 20th January 2015,
Accepted 22nd April 2015

DOI: 10.1039/c5sm00155b

www.rsc.org/softmatter

We drive optically trapped microspheres through entangled F-actin at constant speeds and distances well beyond the linear regime, and measure the microscale force response of the entangled filaments during and following strain. Our results reveal a unique crossover to appreciable nonlinearity at a strain rate of $\dot{\gamma}_c \approx 3\ s^{-1}$ which corresponds remarkably well with the theoretical rate of relaxation of entanglement length deformations $1/\tau_{ent}$. Above $\dot{\gamma}_c$, we observe stress stiffening which occurs over very short time scales comparable to the predicted timescale over which mesh size deformations relax. Stress softening then takes over, yielding to an effectively viscous regime over a timescale comparable to the entanglement length relaxation time, τ_{ent}. The viscous regime displays shear thinning but with a less pronounced viscosity scaling with strain rate compared to flexible polymers. The relaxation of induced force on filaments following strain shows that the relative relaxation proceeds more quickly for increasing strain rates; and for rates greater than $\dot{\gamma}_c$, the relaxation displays a complex power-law dependence on time. Our collective results reveal that molecular-level nonlinear viscoelasticity is driven by non-classical dynamics of individual entanglement segments that are unique to semiflexible polymers.

Introduction

Filamentous actin (F-actin), a semiflexible biopolymer ubiquitous in biological cells, is a key structural protein comprising the cellular cytoskeleton that plays a critical role in important mechanically-driven cellular processes like division, shape change, motility, apoptosis, and many others.[1–6] The versatile biological role of F-actin lies in its unique semiflexible nature, and its ability to form entangled and cross-linked networks that exhibit complex mechanical responses to strain. Beyond the obvious biological relevance, F-actin is also a model semiflexible polymer with a persistence length (l_p) of $\sim$17 μm. This length-scale is comparable to the typical filament length and yields experimentally accessible relaxation dynamics that can reveal molecular-level entangled polymer dynamics.[7–9] As such, the mechanics of F-actin networks have continued to be actively studied for decades.[10,11]

Traditionally, rheology experiments probing the mechanical response of F-actin networks have been on a macroscopic scale and have focused on the linear regime.[10,12–17] More recently, microrheology, which uses embedded microspheres (probes) to sense molecular-level mechanics of soft materials, has emerged as a powerful complementary approach.[18–20] Microrheology can access and directly characterize microscale dynamics that give rise to the macroscopic response by using probes that are either passively diffusing or actively driven *via* magnetic or optical tweezers. Despite the widespread importance of the nonlinear mechanics of F-actin networks, microrheology studies have also focused largely on the linear regime in which results can be interpreted within the well-accepted framework of macrorheology. The few studies that have investigated the nonlinear microscale mechanics, have predominately focused on cross-linked networks.[16,17,21–23] Thus, a molecular-level understanding of the nonlinear response of entangled F-actin to large strains, important to biology, physics and materials science alike, is currently lacking.

The reptation tube model for entangled polymers, pioneered by De Gennes[24] and Doi and Edwards,[25] has been highly successful in describing the mechanical response of entangled polymers to linear strain.[26,27] However, this model, which effectively confines each polymer to a tube-like region surrounding its contour that remains fixed in time and decoupled from any imposed strain, relies on a time-independent uniform density of entanglements. This assumption begins to break down in the nonlinear regime, and several new theories have been proposed that incorporate flow-induced constraint release, tube dilation, chain end retraction, and parallel relaxation mechanisms to account for the reported discrepancies.[27–32] However, the relative

Department of Physics, University of San Diego, 5998 Alcala Park, San Diego, CA 92110, USA. E-mail: randerson@sandiego.edu; Fax: +1-619-260-6874; Tel: +1-619-260-8867

importance of any of these extensions to semiflexible polymers such as F-actin, which can also display unique self-entanglement dampening, potential breakage, buckling, and force propagation over tens of microns remain a topic of debate in the literature.[33,34]

F-actin networks have been shown to display both stress-stiffening and softening (each a nonlinear response to strain) depending on strain magnitude and rate, as well as properties of the network (filament length, concentration, *etc.*).[10,12,16,19,35] However, the molecular-level dynamics and interactions that give rise to this fascinating nonlinear viscoelasticity remain elusive. Stress-stiffening has typically been reported for cross-linked networks in which filaments respond to strain *via* entropic stretching rather than bending which is suppressed by fixed cross-links.[17,22,36] Conversely, it has been suggested that entangled F-actin networks only display stress-softening arising from bending modes dominating the response to strain.[36–39] However, two previous macrorheology experiments have shown evidence of stress-stiffening for entangled F-actin over very short time scales when subject to high strain rates.[16,35]

Here, we use optical tweezers to actively drive probes at constant strain rates through entangled actin and characterize the local (microscale) nonlinear force response of entangled actin filaments during and following strain. With this technique we are able to measure the response with high precision (piconewton forces, nanometer distances, and millisecond times) to characterize the dynamics at the level of individual filaments and entanglements. Our collective results reveal a crossover to distinct non-classical nonlinear dynamics, not previously seen for entangled F-actin, at strain rates higher than the rate of relaxation of individual entanglement segments. This regime is characterized by appreciable stress-stiffening and power-law relaxation that demonstrates that the dynamics of local entanglement constraints dominate the microscale response to nonlinear strain. Our results shed much needed new light into the molecular-level nonlinear mechanical response of entangled F-actin, critical to our understanding of nonlinear cells mechanics as well as entangled semiflexible polymer dynamics.

Materials and methods

Unlabeled rabbit skeletal muscle actin was purchased from Cytoskeleton (AKL99). Fluorescent-labeled Alexa-568 Actin was prepared from acetone powder using the previously described methods from ref. 6 and 40. Actin was stored in Ca Buffer G [2 mM Tris pH 8.0, 0.2 mM ATP, 0.5 mM DTT, 0.1 mM $CaCl_2$] and polymerized in F-buffer [10 mM Imidazole pH 7.0, 50 mM KCl, 1 mM $MgCl_2$, 1 mM EGTA, 0.2 mM ATP]. 4.5 μm carboxylate labeled polystyrene microspheres (probes, Polysciences Inc. #17140) were labeled with Alexa-488 BSA (Invitrogen) to inhibit interaction with the actin network[41] and visualize the probes during measurement.

F-actin networks for experiments were generated by mixing labeled actin, unlabeled actin, and microspheres in F-buffer for a final actin concentration of c_a = 0.5 mg ml^{-1}. At this concentration the mesh size of the network, calculated *via* $\xi = 0.3/c_a^{1/2}$ is ~0.42 μm,[19,42] and the theoretical length between entanglements, l_e, calculated *via* $l_e \sim \xi^{4/5} l_p^{1/5}$, is ~0.89 μm.[43] This mixture was quickly pipetted into a sample chamber constructed with double-sided tape as a spacer between the slide and coverslip and sealed with epoxy. Actin was allowed to polymerize over the course of 30 minutes before measurements, ensuring complete polymerization.[44] Filament length and network uniformity were characterized by imaging the labeled filaments in the network prior to measurements with an Olympus IX70 microscope, which also served as the base for the optical trap. The average filament length was measured to be 7.6 ± 3 μm.

The optical trap was formed by a 1064 nm Nd:YAG fiber laser (Manlight) focused with a 60× 1.4 NA objective (Olympus). A position-sensing detector (Pacific Silicon Sensors) measured the deflection of the trapping laser, which is proportional to the force acting on the trapped probe over our entire force range. The trap stiffness was calibrated *via* Stokes drag in water[45] and passive equipartition methods.[46]

A nanopositioning piezoelectric stage (Mad City Labs) precisely moved the trapped probe 30 μm relative to the sample chamber at speeds of v = 1.5–10 μm s^{-1}. Both stage position and laser deflection data were acquired at 20 kHz during strain and for 15 s following (Fig. 1). Before each measurement, there was a 15 second equilibration period. For each strain speed, 10 different probes were measured with 7 trials per probe at different regions throughout the sample chamber. Displayed data for each speed is an average of all trials. All errors were determined by bootstrapping over 1000 repeating subsets.[47] For ease of interpretation we convert all speeds to strain rates ($\dot{\gamma}$), *via* $\dot{\gamma} = 3v/\sqrt{2}r$ where r is the radius of the probe.[48]

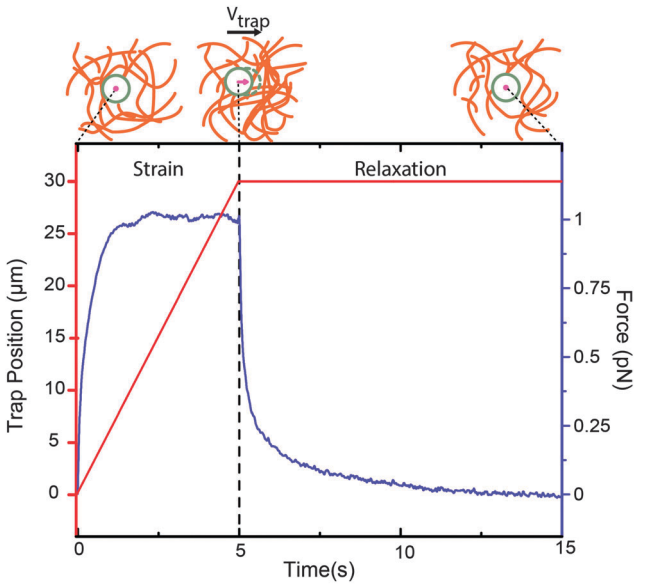

Fig. 1 Experimental setup. The trap position (red, left axis) and measured force on the probe (blue, right axis) are shown for the two phases of the experiment. Strain: after initial equilibration, the trap is displaced 30 μm at a constant rate (6 μm s^{-1} shown) and the force actin filaments exert on the probe is measured. Relaxation: the trap is held constant for 15 seconds and the relaxation of the induced force is measured.

Results & discussion

We find that the force (F) the actin filaments exert on the probe in response to constant rate strains of $\dot{\gamma}$ = 1.41–9.42 s^{-1} initially rises rapidly and later approaches a steady state viscous regime where the force is independent of the strain (Fig. 2A). From the terminal strain-independent force (F_v) we determine the effective viscosity *via* $\eta = F_v/6\pi r\nu$. We find that the viscosity decreases with increasing strain rate following an apparent power law relationship of $\eta \sim \dot{\gamma}^{-1/3}$ (Fig. 2C). This dependence on strain rate has not been observed previously for entangled F-actin, and can be understood to be due to flow-induced release of entanglements (convective constraint release) at high strain rates.[49] Tube model extensions that take into account this phenomena for flexible polymers predict scaling exponents of −0.5 to −1, in line with previous macrorheology experiments on DNA solutions.[50,51] The reduced shear-thinning observed here demonstrates that the semiflexible nature of F-actin leads to more rigid entanglements as compared to traditional flexible polymers due to increased resistance to bending which reduces flow-induced sliding of entanglements.[35]

To characterize the elastic (strain-dependent) approach to the terminal viscous regime, we determine the dependence of the induced force during this approach on strain rate. We normalize the force for each speed by the corresponding terminal regime force (Fig. 2B), and find that the approach to the viscous regime is strain rate dependent, with increasing rates approaching the viscous regime more slowly. We quantify the strain distance at which the force has reached 90% of its terminal regime value as the yield distance (d_y) and find that the yield distance increases linearly with strain rate. The slope of yield distance d_y *vs.* speed v gives a rate-independent yield time of $t_y \approx 0.29$ s. This yield time is comparable to the theoretical timescale for entanglement length relaxations $\tau_{ent} \approx 0.23$ s for 0.5 mg ml^{-1} entangled F-actin[52] indicating that the microscale elastic regime is driven by individual deformed entanglement segments (Fig. 2B inset and D).

To further characterize the initial elastic regime, we calculate the differential modulus K ($K = dF/dx$, Fig. 3A), analogous to an effective spring constant, that quantifies the stiffness of the network. We find that for all speeds the actin network initially stiffens (with K increasing from its initial value K_0 to a peak value K_{max}, Fig. 3B), followed by a period of softening to the terminal viscous regime (where $K \approx 0$). Examined as a function of time, K collapses onto a single curve for all strain rates

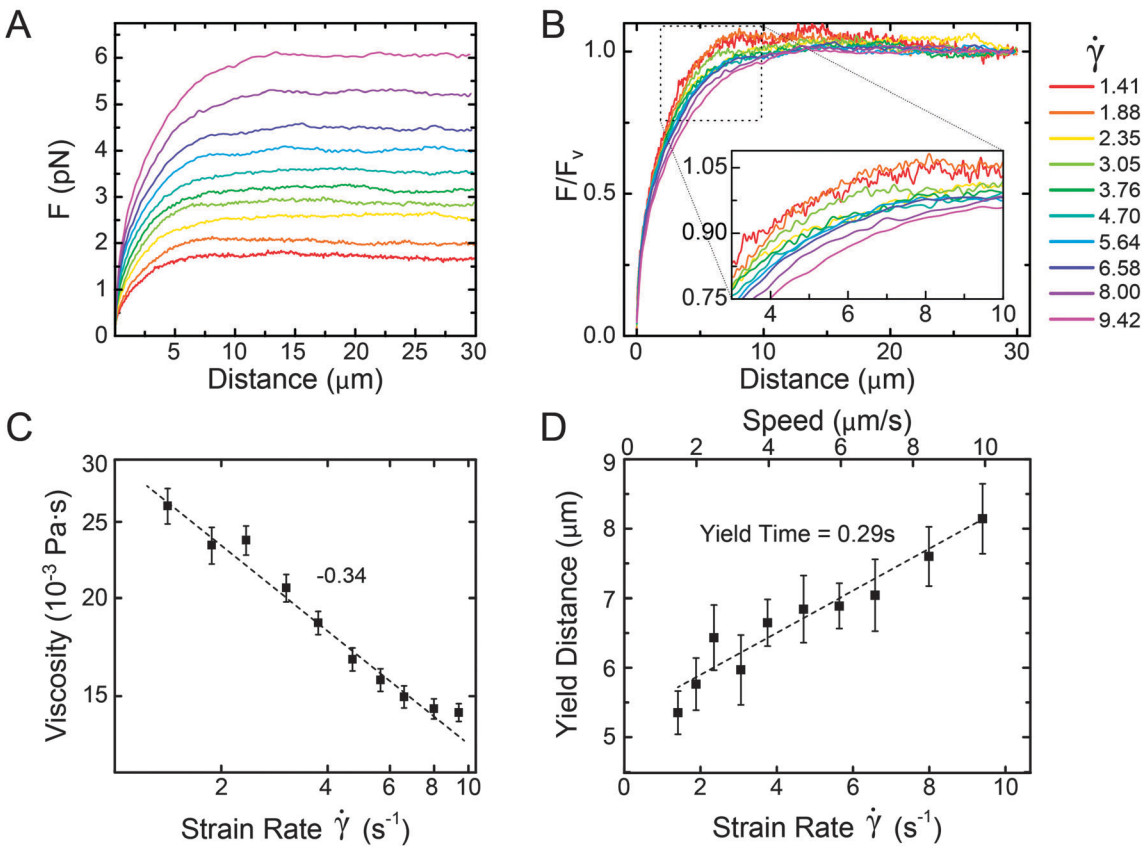

Fig. 2 Nonlinear microscale force response of actin filaments during strain. (A) Measured force F on probe during strain for strain rates $\dot{\gamma}$ of 1.4 to 9.4 s^{-1} (listed in legend in B) (B) measured force for each strain rate normalized by the corresponding force in the terminal viscous regime (F_v). Inset: zoomed view during yielding transition from strain-dependent (elastic) to strain-independent (viscous) regime (C) effective viscosity in the terminal regime, calculated from F_v, as a function of strain rate. Dashed line shows apparent power law scaling with a measured exponent of −0.34 quantifying the degree of shear-thinning. (D) Yield distance as a function of strain rate (and speed). Dashed line is a linear fit to the data with a slope of 0.29 s that quantifies the measured yield time.

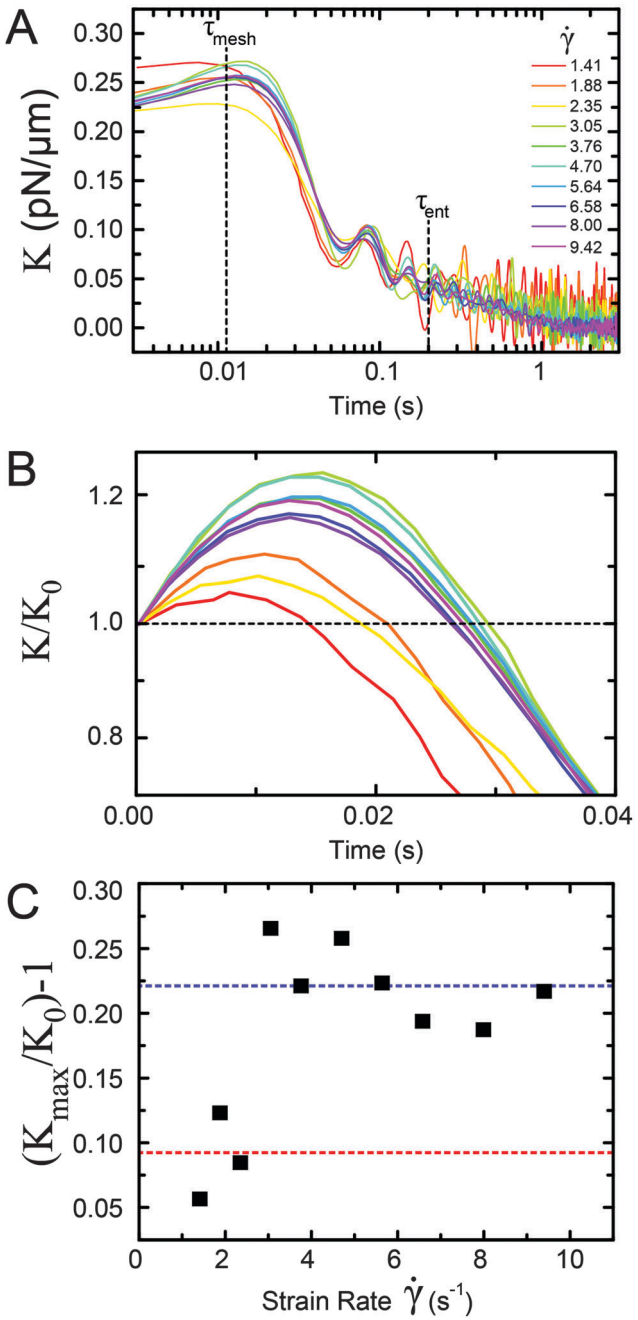

Fig. 3 Differential modulus K of the force response during strain. (A) Differential modulus $K = dF/dx$ (pN μm^{-1}) as a function of time (s) for strain rates $\dot{\gamma}$ of 1.4 to 9.4 s^{-1} (listed in legend). Theoretical timescales for the relaxation of mesh size (τ_{mesh}) and entanglement length (τ_{ent}) deformations (B) K for each strain rate normalized by the corresponding initial value K_0 as a function of time showing relative stress-stiffening to a maximum value K_{max} followed by stress-softening (C) degree of stress-stiffening, quantified by $K_{max}/K_0 - 1$, as a function of strain rate. Dashed lines correspond to the average stiffening degree for strain rates below (red, $K_{max}/K_0 - 1 \approx 8\%$) and above (blue, $K_{max}/K_0 - 1 \approx 22\%$) the crossover rate of 3 s^{-1}.

showing that the timescale over which K stiffens and subsequently softens is independent of strain rate (Fig. 3A). As demonstrated in Fig. 3A, the timescale over which the local network maintains or increases its initial stiffness is ~0.012 s, which is remarkably close to the theoretical timescale over which deformations on the order of the mesh size are able to relax ($\tau_{mesh} \approx 0.012$ s for 0.5 mg ml^{-1} entangled F-actin).[52] Because the mesh size is the smallest characteristic lengthscale of the network, no viscoelastic dissipation is able to occur until this lengthscale has been able to relax. For times shorter than this relaxation time, the network is instead forced to stiffen is response to an imposed strain. As stiffening has been shown to arise from entropic filament stretching and suppressed bending,[22] our results indicate that substantial bending of filaments can only occur over length scales greater than the mesh size. In accord with our yield time analysis, we see that complete softening to $K \approx 0$ occurs over a timescale comparable to the entanglement length relaxation time (Fig. 3A), once again demonstrating that elasticity is driven by individual entanglement segments.

While the timescale for stiffening and softening appears independent of strain rate, the degree of stiffening (*i.e.* $K_{max}/K_0 - 1$) displays a strain rate dependent crossover from negligible to appreciable stiffening (Fig. 3C). For strain rates below ~3 s^{-1} the average degree of stiffening is ~8% while for $\dot{\gamma} > 3$ s^{-1} we find ~22% stiffening. This crossover strain rate $\dot{\gamma}_c \approx 3$ s^{-1} is nearly identical to our measured yielding rate ($1/t_y$) as well as the rate for entanglement length relaxations to relax ($1/\tau_e$). Thus, stiffening of entangled actin networks is only induced when the strain is fast enough that individual entanglement length segments are unable to relax on the timescale of the strain (*i.e.* when $\dot{\gamma} > 1/\tau_e$). This finding helps to resolve the current debate in the literature (discussed in the Introduction) regarding whether sterically entangled F-actin networks are able to display stiffening or only softening during strain.

We also measure the relaxation of induced force following strain, which we find exhibits a complex dependence on strain rate (Fig. 4). The relative force dissipation following strain (F/F_0) actually proceeds more quickly for higher strain rates, and the time-dependence of the force relaxation is distinctly different for strain rates above and below $\dot{\gamma}_c \approx 3$ s^{-1}. For rates below ~3 s^{-1} the relaxations are well fit to a double exponential function of time with average decay times of ~0.25 s and ~2.5 s, indicating two distinct relaxations mechanisms. The first decay time is simply the relaxation time for entanglement segments τ_{ent} showing once again the dominant role that individual entanglements play in the microscale force response. The longer timescale is more difficult to interpret. Theoretically, the relaxation mechanism and corresponding timescale that follows entanglement segment relaxation is the relaxation of the entanglement tube with an associated timescale τ_{tube} which is predicted to be ~17 s for our system.[52] However, all theoretical timescales rely on the assumption that the tube size is fixed in time. If our longer relaxation timescale is indeed due to tube relaxation, as predicted, our measured decay time of $\sim \tau_{tube}/6$ indicates that the tube has dilated from its initial size. In other words the entanglement density has been reduced from its equilibrium value, enabling faster relaxation of the deformed tube. Nonetheless, an exponential relaxation with well-separated timescales, indicative of a linear response within the classical tube theory framework, suggests that

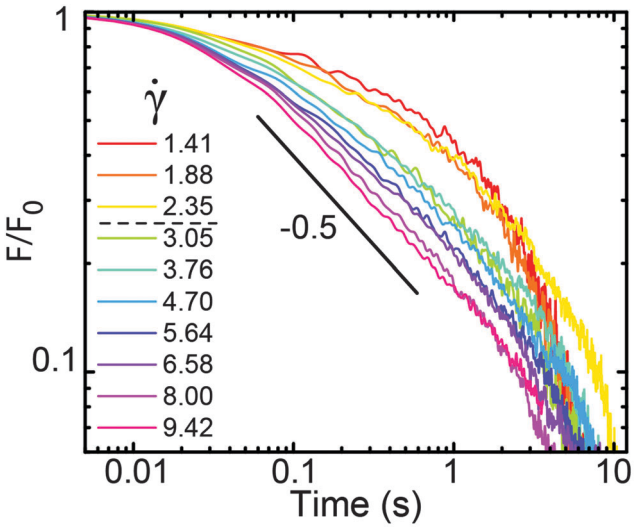

Fig. 4 Relaxation of induced force following strain. Measured force F normalized by the corresponding initial value F_0, as a function of time (s) during the relaxation phase of the experiment for strain rates $\dot{\gamma}$ of 1.4 to 9.4 s^{-1} (listed in legend). The dashed line separates strain rates below and above the crossover rate of $\sim 3\ s^{-1}$. The solid line corresponds to a power law time decay of force ($F \sim t^{-b}$) with a scaling exponent $b = -0.5$ for $\dot{\gamma} > 3\ s^{-1}$.

the tube size, while dilated, is relatively fixed in time, and not directly coupled to the induced strain.[26,52] Conversely, rates above $\sim 3\ s^{-1}$ exhibit power law stress decay ($F \sim \tau^{-b}$), following a very brief initial phase of minimal relaxation, with an apparent scaling exponent of $b \sim -0.5$. Two-phase power-law force relaxation has been recently predicted by Sussman and Schweizer[28,29] and understood to be due to (i) classical relaxation of a deformed entanglement tube which has been dilated by the strain; coupled with (ii) healing of the dilated tube back to its equilibrium classical size. Thus, initial relaxation proceeds more quickly because the tube is dilated from its equilibrium size, and power-law decay arises from the tube relaxation timescale increasing with time as $\tau_{tube} \sim t^{0.6}$ as it heals (or contracts) back to its original size.[28,29] Thus, while our $\dot{\gamma} < 3\ s^{-1}$ results show evidence of tube dilation, force relaxations for $\dot{\gamma} > 3\ s^{-1}$ indicate more extreme dilation and complex healing as a result of non-classical entanglements that are coupled to the induced stress.[28,29] Tube dilation can also be understood as due to entanglement density reduction by non-affine deformation of tube constraints as suggested previously for entangled F-actin.[28]

Thus, our results show a strain-rate dependent crossover to appreciable stress-stiffening during strain and power-law stress relaxation following strain, both nonlinear responses not predicted by classical entanglement theory. This crossover, not previously observed or predicted for entangled actin, occurs at $\dot{\gamma}_c \approx 3\ s^{-1}$ and reveals that the dominant relaxation mechanism that controls nonlinear behavior occurs on a timescale of $\tau_c \approx 0.3$ s, quite close to the predicted relaxation time for individual entanglements ($\tau_{ent} \approx 0.23$ s).[52] Thus, our collective results reveal that nonlinearity at the molecular-level is induced by individual entanglement segments that are unable to relax on the timescale of the strain.

Conclusion

In summary, we use optical tweezers microrheology to characterize the microscale nonlinear mechanical response of entangled actin filaments. Our results reveal a unique crossover to nonlinear dynamics for strain rates faster than the rate of relaxation of individual entanglement segments. In this regime, when subject to strain, we find that the entangled filaments initially stiffen due to inhibited relaxation of lengthscales greater than the mesh size, which prohibits bending of filaments. Stress-softening is induced when individual deformed entanglement segments are able to release stress, likely by bending. Once entanglement segments have relaxed, entangled filaments behave effectively fluid with modest shear thinning, unique to entangled F-actin, due to release of entanglements. Microscale force relaxation following strain indicates dynamic strain-induced entanglement tube dilation and healing, corroborating very recent theoretical predictions for the first time.[28,29] Thus, our collective results reveal the microscale dynamics that give rise to the macroscopic nonlinear mechanical response of entangled semi-flexible polymers, and can be used to understand the complex nonlinear mechanics of biological cells.

Acknowledgements

This research was funded by an NSF CAREER Award, grant number 1255446. We would also like to thank Cole E. Chapman for assistance with the optical trap and Robert Fitzpatrick for contributions to length distribution measurements.

References

1 E. S. Chhabra and H. N. Higgs, *Nat. Cell Biol.*, 2007, **9**, 1110–1121.
2 B. J. Galletta and J. A. Cooper, *Curr. Opin. Cell Biol.*, 2009, **21**, 20–27.
3 M. Kaksonen, C. P. Toret and D. G. Drubin, *Nat. Rev. Mol. Cell Biol.*, 2006, **7**, 404–414.
4 A. J. Ridley, M. A. Schwartz, K. Burridge, R. A. Firtel, M. H. Ginsberg, G. Borisy, J. T. Parsons and A. R. Horwitz, *Science*, 2003, **302**, 1704–1709.
5 J. Q. Wu, J. R. Kuhn, D. R. Kovar and T. D. Pollard, *Dev. Cell*, 2003, **5**, 723–734.
6 D. R. Kovar, J. R. Kuhn, A. L. Tichy and T. D. Pollard, *J. Cell Biol.*, 2003, **161**, 875.
7 A. Ott, M. Magnasco, A. Simon and A. Libchaber, *Phys. Rev. E: Stat. Phys., Plasmas, Fluids, Relat. Interdiscip. Top.*, 1993, **48**, R1642.
8 F. Gittes, B. Mickey, J. Nettleton and J. Howard, *J. Cell Biol.*, 1993, **120**, 923–934.
9 B. Wang, J. Guan, S. M. Anthony, S. C. Bae, K. S. Schweizer and S. Granick, *Phys. Rev. Lett.*, 2010, **104**, 118301.
10 J. Stricker, T. Falzone and M. L. Gardel, *J. Biomech.*, 2010, **43**, 9–14.
11 R. Dominguez and K. C. Holmes, *Annu. Rev. Biophys.*, 2011, **40**, 169.

12 P. A. Janmey, S. Hvidt, J. Käs, D. Lerche, A. Maggs, E. Sackmann, M. Schliwa and T. P. Stossel, *J. Biol. Chem.*, 1994, **269**, 32503–32513.
13 J. Käs, H. Strey, J. Tang, D. Finger, R. Ezzell, E. Sackmann and P. Janmey, *Biophys. J.*, 1996, **70**, 609–625.
14 G. Koenderink, M. Atakhorrami, F. MacKintosh and C. Schmidt, *Phys. Rev. Lett.*, 2006, **96**, 138307.
15 H. Hinsch, E. Frey, arXiv preprint arXiv, 0907.1875, 2009.
16 C. Semmrich, R. J. Larsen and A. R. Bausch, *Soft Matter*, 2008, **4**, 1675–1680.
17 J. Liu, G. Koenderink, K. Kasza, F. MacKintosh and D. Weitz, *Phys. Rev. Lett.*, 2007, **98**, 198304.
18 T. G. Mason and D. A. Weitz, *Phys. Rev. Lett.*, 1995, **74**, 1250.
19 M. Gardel, M. Valentine, J. C. Crocker, A. Bausch and D. Weitz, *Phys. Rev. Lett.*, 2003, **91**, 158302.
20 J. Liu, M. L. Gardel, K. Kroy, E. Frey, B. D. Hoffman, J. C. Crocker, A. R. Bausch and D. A. Weitz, *Phys. Rev. Lett.*, 2006, **96**, 118104.
21 O. Chaudhuri, S. H. Parekh and D. A. Fletcher, *Nature*, 2007, **445**, 295–298.
22 M. Gardel, J. Shin, F. MacKintosh, L. Mahadevan, P. Matsudaira and D. Weitz, *Science*, 2004, **304**, 1301–1305.
23 R. Tharmann, M. Claessens and A. Bausch, *Phys. Rev. Lett.*, 2007, **98**, 088103.
24 M. Doi and S. Edwards, *The Theory of Polymer Dynamics*, Clarendon, Oxford, 1986, ISBN 0-19-852033-6.
25 P.-G. De Gennes, *Scaling concepts in polymer physics*, Cornell university press, 1979.
26 R. M. Robertson and D. E. Smith, *Phys. Rev. Lett.*, 2007, **99**, 126001.
27 S.-Q. Wang, S. Ravindranath, Y. Wang and P. Boukany, *J. Chem. Phys.*, 2007, **127**, 064903.
28 D. M. Sussman and K. S. Schweizer, *Macromolecules*, 2012, **45**, 3270–3284.
29 D. M. Sussman and K. S. Schweizer, *Macromolecules*, 2013, **46**, 5684–5693.
30 R. S. Graham, A. E. Likhtman, T. C. McLeish and S. T. Milner, *J. Rheol.*, 2003, **47**, 1171–1200.
31 G. Marrucci, *J. Non-Newtonian Fluid Mech.*, 1996, **62**, 279–289.
32 D. M. Sussman and K. S. Schweizer, *Phys. Rev. Lett.*, 2011, **107**, 078102.
33 R. G. Larson, *J. Polym. Sci., Part B: Polym. Phys.*, 2007, **45**, 3240–3248.
34 A. E. Likhtman, *J. Non-Newtonian Fluid Mech.*, 2009, **157**, 158–161.
35 J. Xu, Y. Tseng and D. Wirtz, *J. Biol. Chem.*, 2000, **275**, 35886–35892.
36 K. Kroy and E. Frey, *Phys. Rev. Lett.*, 1996, **77**, 306.
37 J. Wilhelm and E. Frey, *Phys. Rev. Lett.*, 2003, **91**, 108103.
38 D. A. Head, A. J. Levine and F. MacKintosh, *Phys. Rev. Lett.*, 2003, **91**, 108102.
39 D. Head, A. Levine and F. MacKintosh, *Phys. Rev. E: Stat. Phys., Plasmas, Fluids, Relat. Interdiscip. Top.*, 2003, **68**, 061907.
40 J. R. Kuhn and T. D. Pollard, *Biophys. J.*, 2005, **88**, 1387–1402.
41 M. T. Valentine, Z. E. Perlman, M. L. Gardel, J. H. Shin, P. Matsudaira, T. J. Mitchison and D. A. Weitz, *Biophys. J.*, 2004, **86**, 4004–4014.
42 C. F. Schmidt, M. Baermann, G. Isenberg and E. Sackmann, *Macromolecules*, 1989, **22**, 3638–3649.
43 A. N. Semenov, *J. Chem. Soc., Faraday Trans. 2*, 1986, **82**, 317–329.
44 L. S. Tobacman and E. D. Korn, *J. Biol. Chem.*, 1983, **258**, 3207–3214.
45 P. Wissenburg, T. Odijk, P. Cirkel and M. Mandel, *Macromolecules*, 1995, **28**, 2315–2328.
46 C. D. Chapman and R. M. Robertson-Anderson, *Phys. Rev. Lett.*, 2014, **113**, 098303.
47 B. Efron, *Biometrika*, 1981, **68**, 589–599.
48 T. M. Squires, *Langmuir*, 2008, **24**, 1147–1159.
49 Y. Lu, L. An, S.-Q. Wang and Z.-G. Wang, *ACS Macro Lett.*, 2014, **3**, 569–573.
50 R. E. Teixeira, A. K. Dambal, D. H. Richter, E. S. Shaqfeh and S. Chu, *Macromolecules*, 2007, **40**, 2461–2476.
51 P. S. Desai and R. G. Larson, *J. Rheol.*, 2014, **58**, 255–279.
52 H. Isambert and A. Maggs, *Macromolecules*, 1996, **29**, 1036–1040.

